ACS central science

Research Article

http://pubs.acs.org/journal/acscii

Reinventing Cell Penetrating Peptides Using Glycosylated Methionine Sulfonium Ion Sequences

Jessica R. Kramer,[†,‡] Nathan W. Schmidt,[‡,§] Kristine M. Mayle,[§] Daniel T. Kamei,[§] Gerard C. L. Wong,[†,§] and Timothy J. Deming*[,†,§]

[§]Department of Bioengineering and [†]Department of Chemistry and Biochemistry, University of California, Los Angeles, California 90095, United States

Supporting Information

ABSTRACT: Cell penetrating peptides (CPPs) are intriguing molecules that have received much attention, both in terms of mechanistic analysis and as transporters for intracellular therapeutic delivery. Most CPPs contain an abundance of cationic charged residues, typically arginine, where the amino acid compositions, rather than specific sequences, tend to determine their ability to enter cells. Hydrophobic residues are often added to cationic sequences to create efficient CPPs, but typically at the penalty of increased cytotoxicity. Here, we examined polypeptides containing glycosylated, cationic derivatives of methionine, where we found these hydrophilic polypeptides to be surprisingly effective as CPPs and to also possess low cytotoxicity. X-ray analysis of how these new polypeptides interact with lipid membranes revealed that the incorporation of sterically demanding hydrophilic cationic groups in polypeptides is an unprecedented new concept for design of potent CPPs.

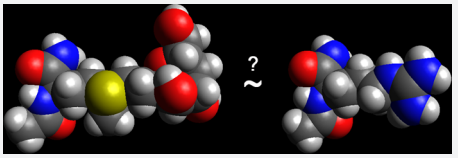

INTRODUCTION

Many natural cell penetrating peptides (CPPs) and synthetic CPP mimics are based on molecules containing multiple guanidinium groups, where the specific H-bonding properties of guanidinium ions impart these molecules with the ability to cross cell membranes.[1−3] In the case of poly(arginine), cell uptake is maximal when chains are approximately 9 to 15 residues long, while longer chains show progressively diminished cell uptake and increased cytotoxicity.[4,5] The significance of poly(arginine) H-bonding and chain length in determining CPP activity was found to arise from packing of multiple guanidinium groups. Recent X-ray experiments, in conjunction with QM and MD simulations,[6] have shown that the multivalent H-bonding of guanidinium allows it to strongly interact with multiple lipid components thereby causing poly(arginine) to generate saddle-shaped, negative Gaussian curvature (positive and negative curvature in orthogonal directions, *vide infra*), which is geometrically necessary for membrane translocation events such as pore formation as well as invaginated morphologies that occur during endocytosis.[5−8] These results suggest that the paradigm for CPP design requires molecules containing multiple functional groups that will generate negative Gaussian curvature in lipid membranes, as currently best exemplified by poly(guanidinium) species.

Other polycationic molecules that lack guanidinium groups, such as poly(lysine), are typically poor CPPs since they can only generate cylinder-shaped, negative mean curvature (*vide infra*), which is a necessary but insufficient condition for negative Gaussian curvature.[7,8] The CPP activity of such molecules can be improved through incorporation of hydrophobic groups that generate positive curvature by inserting into lipid membranes, where the resulting combination of negative and positive curvature results in negative Gaussian curvature.[6,8,9] Such cationic and hydrophobic molecules can be efficient CPPs, yet they typically show higher cytotoxicity compared to poly(guanidinium) molecules lacking hydrophobic groups.[6,9] While there have been significant recent advances in the development of cell transporter polymers containing diverse cationic groups that include guanidinium,[10] phosphonium,[11,12] and sulfonium,[13] all of these materials behave according to the principles described above. Namely, incorporation of hydrophobic groups leads to increased cell transporter activity and increased cytotoxicity, while incorporation of hydrophilic groups decreases cytotoxicity, but also decreases or does not improve cell transporter activity.[14] At present, there are no CPPs that circumvent this trade-off.

Realizing that negative Gaussian curvature generation in membranes is a characteristic of all CPP molecules,[6,7] and that this property may be achieved via different molecular structures, we reasoned that other chemical motifs beyond guanidinium may be effective, or even superior, at generating this type of curvature. To test this idea, we used our recently reported method of methionine alkylation for facile introduction of different chemical functional groups in polypeptides to obtain a variety of stable sulfonium containing polypeptides as new candidate CPPs.[15] These sulfonium cations, unlike guanidinium groups, are distinct in that they cannot use H-bonding to induce membrane curvature. These methionine functionalizations are simple reactions that are compatible with many functional groups, use an inexpensive, natural amino acid, and, as with CPPs, utilize a degradable peptide backbone.[16,17] Furthermore, alkylated poly(methionine) sulfoniums are polycationic species, which is a

Received: February 23, 2015
Published: April 15, 2015

DOI: 10.1021/acscentsci.5b00054
ACS Cent. Sci. 2015, 1, 83−88

critical requirement for strong membrane binding in CPPs.[18] Our objective was to use poly(methionine) sulfoniums as a new peptide platform to test the ability of different cationic groups to impart cell penetrating properties.

RESULTS AND DISCUSSION

We prepared a number of poly(L-methionine) derivatives ($\mathbf{M}^{\mathbf{R}}_{n}$) that varied in chain length (n), added functionality (R), and degree of alkylation (x) (Figure 1). Using literature methods,[17]

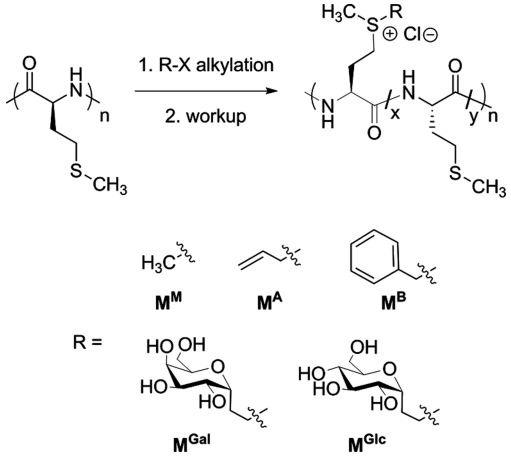

Figure 1. Synthesis of cationic poly(L-methionine) derivatives ($\mathbf{M}^{\mathbf{R}}_{n}$) using different alkylating reagents (R–X, X = Br, OTf). n = degree of polymerization. x, y = mole fractions of different residue types.

poly(L-methionine) chains were prepared with average lengths ranging from 10 to 60 residues (see Table S1). These chains were then reacted with alkylating reagents in different quantities (see Table S2), to obtain the functionalized polypeptides shown in Figure 1.[15] All glycosylated $\mathbf{M}^{\mathbf{R}}_{n}$ polypeptides studied were water-soluble and adopted disordered conformations in solution, except for derivatives that were less than 50 mol % modified, which were partially α-helical and showed diminished solubility (see Figure S1). $\mathbf{M}^{\mathbf{R}}_{n}$ polypeptides alkylated with hydrophobic groups were water soluble only when near 100 mol % modified. We chose the alkylating functional groups to include a neutral methyl group, hydrophobic allyl and benzyl groups, and hydrophilic monosaccharides. These functional groups were chosen to obtain cationic sulfonium groups that varied from hydrophobic to hydrophilic for evaluation of their cytotoxicity and cell uptake ability.

Initial studies on 100 mol % hydrophobically modified polypeptides $\mathbf{M}^{\mathbf{M}}_{60}$, $\mathbf{M}^{\mathbf{A}}_{60}$, and $\mathbf{M}^{\mathbf{B}}_{60}$ revealed that these samples were toxic at elevated concentrations to PC3 cells, a prostate cancer cell line (see Figure S2). In this assay, the nona-arginine peptide, $\mathbf{R}_9$, was minimally toxic at the concentrations tested, while a longer poly(L-homoarginine)$_{60}$, $\mathbf{R}_{60}$, showed marked toxicity, which is likely due to its long chain length and high density of cationic groups.[4−6] The least hydrophobic sample, $\mathbf{M}^{\mathbf{M}}_{60}$, was the least toxic of the three, which encouraged testing of the more hydrophilic $\mathbf{M}^{\mathbf{Gal}}$ and $\mathbf{M}^{\mathbf{Glc}}$ polypeptides in an effort to identify samples with good cell compatibility. PC3 cell viability studies were next carried out using $\mathbf{M}^{\mathbf{Gal}}_{10}$ and $\mathbf{M}^{\mathbf{Gal}}_{60}$ polypeptides that, due to their good water solubility, could be either 50 mol % or 100 mol % glycosylated for each length (Figure 2). The hydrophilic, 100% glycosylated $\mathbf{M}^{\mathbf{Gal}}_{60}$ was also quite toxic at elevated concentrations, likely for reasons similar to those for longer $\mathbf{R}_{60}$. The shorter 100% glycosylated $\mathbf{M}^{\mathbf{Gal}}_{10}$ was

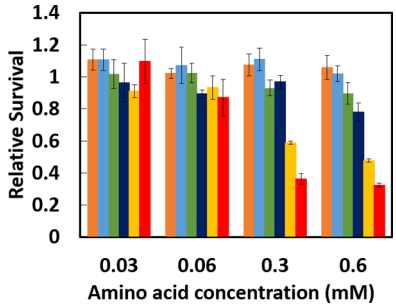

Figure 2. Relative survival of PC3 cells incubated for 5 h with polypeptide samples. Polypeptides studied were $\mathbf{R}_9$ (orange), 50% $\mathbf{M}^{\mathbf{Gal}}_{10}$ (light blue), 100% $\mathbf{M}^{\mathbf{Gal}}_{10}$ (green), 50% $\mathbf{M}^{\mathbf{Gal}}_{60}$ (dark blue), 100% $\mathbf{M}^{\mathbf{Gal}}_{60}$ (yellow), and $\mathbf{R}_{60}$ (red). Cell survival was determined using the MTS assay, and amino acid concentrations were used in order to equate samples with different chain lengths. Error bars represent the standard deviation from an average of three measurements.

only marginally toxic compared to similar length $\mathbf{R}_9$. The 50% glycosylated $\mathbf{M}^{\mathbf{Gal}}$ polypeptides were found to be less cytotoxic compared to corresponding 100% glycosylated versions, with 50% $\mathbf{M}^{\mathbf{Gal}}_{10}$ showing negligible toxicity similar to that of $\mathbf{R}_9$ (Figure 2). In the 50% glycosylated samples, improved cell compatibility is likely due to fewer cationic groups, even though these were replaced with hydrophobic methionine residues that normally would be expected to increase cytotoxicity.[9] The corresponding $\mathbf{M}^{\mathbf{Glc}}$ polypeptides gave PC3 cell viabilities that were similar to those of the $\mathbf{M}^{\mathbf{Gal}}$ samples.

Our cell viability studies showed that glycosylated and methylated polypeptides ($\mathbf{M}^{\mathbf{Gal}}$, $\mathbf{M}^{\mathbf{Glc}}$, and $\mathbf{M}^{\mathbf{M}}$) were the most promising for further evaluation. Initial experiments in PC3 cells comparing cell uptake of 100% functionalized $\mathbf{M}^{\mathbf{M}}_{60}$ and 100% $\mathbf{M}^{\mathbf{Gal}}_{60}$ revealed that these samples differed greatly, with 100% $\mathbf{M}^{\mathbf{Gal}}_{60}$ possessing far superior uptake properties (see Figure S3). Focusing on the $\mathbf{M}^{\mathbf{Gal}}$ samples, we varied their degree of glycosylation from 100 to 50%, and also their average chain length from 10 to 60 residues to see how cell uptake properties were affected. We found that decreasing glycosylation from 100 to 50%, regardless of chain length, correlated with improved cell uptake (see Figure S4), and that chain length variation for 50% $\mathbf{M}^{\mathbf{Gal}}$ samples had a minimal effect on cell uptake (see Figure S5). These intriguing results showed that 50% $\mathbf{M}^{\mathbf{Gal}}_{10}$ possesses an optimal combination of minimal cytotoxicity and high cell uptake, and warranted further evaluation as a CPP.

We compared 50% $\mathbf{M}^{\mathbf{Gal}}_{10}$ against the benchmark CPP $\mathbf{R}_9$, which also has low toxicity and excellent cell uptake properties. Different concentrations of fluorescently labeled 50% $\mathbf{M}^{\mathbf{Gal}}_{10}$ or $\mathbf{R}_9$ (ca. 1 mol % label per residue) were incubated with PC3 cells for 1 h in serum free medium, followed by imaging using laser scanning confocal microscopy (LSCM) (Figure 3, see Figure S6) and differential interference contrast (DIC) microscopy (see Figure S7). At all concentrations, 50% $\mathbf{M}^{\mathbf{Gal}}_{10}$ showed significantly greater cell uptake compared to $\mathbf{R}_9$, and especially proved to be a more efficient CPP at lower peptide concentrations (Figure 3G). Note that both samples showed similar types of uptake in these cells including both punctate and diffuse fluorescence within the cell bodies. Excellent uptake was also found in HeLa cells for 50% $\mathbf{M}^{\mathbf{Gal}}_{10}$, showing that its CPP activity is not specific to a single cell type (see Figure S8). Comparison of 50% $\mathbf{M}^{\mathbf{Gal}}_{10}$ and 50% $\mathbf{M}^{\mathbf{Glc}}_{10}$ further showed that the specific monosaccharide was not important as both samples had similar uptake in PC3 cells (see Figure S9). Specific

DOI: 10.1021/acscentsci.5b00054
ACS Cent. Sci. 2015, 1, 83−88

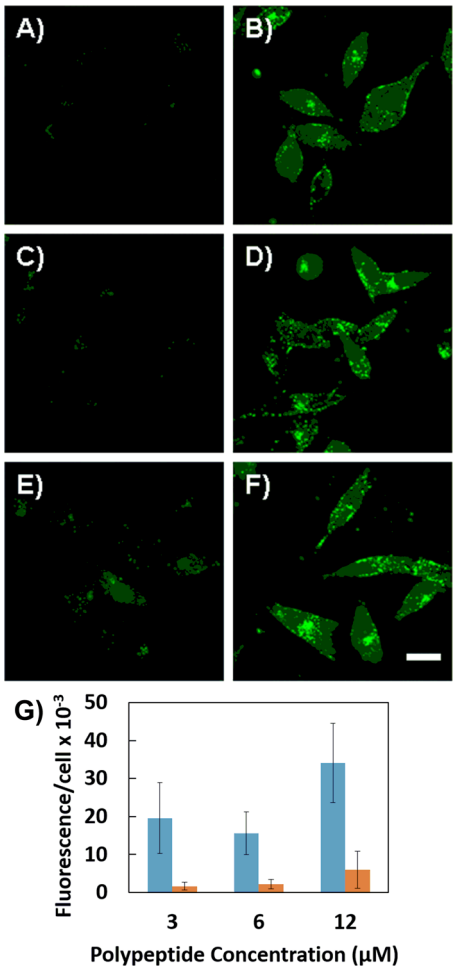

Figure 3. LSCM images showing concentration dependent polypeptide uptake in PC3 cells. Cells were incubated with solutions of fluorescein labeled $\mathbf{R}_9$ peptide (A, C, E) or 50% $\mathbf{M}^{\mathbf{Gal}}{}_{10}$ (B, D, F). LSCM images of cells incubated for 1 h with polypeptide concentrations of (A, B) 3 μM, (C, D) 6 μM, or (E, F) 12 μM. Samples at each concentration had equivalent fluorescence emission intensities, with ca. 1 label per 100 residues (see Figure S6). 3 μM polypeptide is equivalent to 0.03 mM amino acid for these samples. Scale bar = 25 μm. (G) Fluorescence quantification was performed using ImageJ software. The corrected total fluorescence per cell (fluorescence/cell) was found to be significantly different between 50% $\mathbf{M}^{\mathbf{Gal}}{}_{10}$ (light blue) and $\mathbf{R}_9$ (orange) at all concentrations (two-way ANOVA on peptide type and concentration, $p < 0.001$ for both factors; post hoc Tukey's honest significant difference (HSD) test for 50% $\mathbf{M}^{\mathbf{Gal}}{}_{10}$ vs $\mathbf{R}_9$, $p < 0.05$).

interaction of the monosaccharides in 50% $\mathbf{M}^{\mathbf{Gal}}{}_{10}$ with cell surfaces was also ruled out by competition experiments using a large excess of free galactose, which did not diminish polypeptide cell uptake (see Figure S10). These data confirm that the 50% glycosylated polypeptides have characteristics of highly effective CPPs, where the cationic glycosylated residues appear to be an important contributor to their activity.

In order to better understand how the different molecular features of these cationic glycosylated polypeptides give rise to CPP activity, we studied the interactions of these materials with small unilamellar lipid vesicle formulations (SUVs) (see Figure S11) using synchrotron small-angle X-ray scattering (SAXS). SUVs were composed of ternary compositions of DOPE/DOPC/DOPS lipids in order to assay how the curvatures generated by $\mathbf{M}^{\mathbf{Gal}}$ samples varied over a range of physiologically relevant membrane conditions.[5−7] Specifically, we mapped out the effects of monolayer spontaneous curvature on $\mathbf{M}^{\mathbf{Gal}}$ phase behavior by fixing the concentration of anionic DOPS (spontaneous curvature, $c_0 \approx 0$) at 20%, and varying the ratio of DOPE ($c_0 < 0$) and DOPC ($c_0 \approx 0$) in the membrane.[19] We first studied fully glycosylated samples and found that 100% $\mathbf{M}^{\mathbf{Gal}}{}_{10}$ generated a polymorphism of lipid phases over a wide range of membrane DOPE content (Figure 4A,B). At peptide to lipid (P/L) = 1/50, in DOPE/DOPS = 80/20 membranes enriched in negative spontaneous curvature lipids, reflections were observed at Q-positions with characteristic ratios $1:\sqrt{3}:2:\sqrt{7}$, indicating that 100% $\mathbf{M}^{\mathbf{Gal}}{}_{10}$, similar to other polycations, induced an inverted hexagonal phase with negative mean curvature (Figure 4E). With 70% and 60% DOPE membranes, in addition to the hexagonal phase, a second set of reflections were also present, with ratios $\sqrt{2}:\sqrt{3}:\sqrt{4}:\sqrt{6}$, from a coexisting *Pn*3*m* cubic phase characterized by negative Gaussian curvature at every point (Figure 4A,B,E). Lattice parameters for all the phases are compiled in Table S3. The nonlamellar cubic and inverted hexagonal phases persist until 40% DOPE, where reflections with integral Q-position ratios are observed from a lamellar phase with zero curvature (Figure 4E). As observed with other CPPs,[5−7] the phases induced by 100% $\mathbf{M}^{\mathbf{Gal}}{}_{10}$ strongly depend on the concentration of negative spontaneous curvature lipids in the membrane.

The effect of polymer length on curvature generation was dramatic (Figure 4C,D), as use of 6-fold longer 100% $\mathbf{M}^{\mathbf{Gal}}{}_{60}$ led to a substantial decrease in nonlamellar phase formation. In DOPE/DOPS = 80/20 membranes at P/L = 1/450, 100% $\mathbf{M}^{\mathbf{Gal}}{}_{60}$ induced coexisting nonlamellar *Pn*3*m* cubic and inverted hexagonal phases. However, in membranes with ≤70% DOPE content, only lamellar phases were observed (Figure 4C,D). This behavior differs substantially from 100% $\mathbf{M}^{\mathbf{Gal}}{}_{10}$, which induced cubic and inverted hexagonal phases at much lower DOPE content. A similar trend was also found to hold for 50% $\mathbf{M}^{\mathbf{Gal}}{}_{60}$ (see Figure S12), indicating that polypeptide length is an important factor for curvature generation in membranes. This phenomenon is similar to that observed for different length poly(arginine)s, where cumulative molecular crowding from arranging many cationic groups along the peptide chain generates a large positive curvature strain, which can interfere with the negative curvature component and limit the generation of negative Gaussian curvature.[5,6]

To determine the effects of reduced polypeptide glycosylation on membrane curvature generation, we conducted SAXS measurements using 50% $\mathbf{M}^{\mathbf{Gal}}{}_{10}$. Overall, the phase behavior for 50% $\mathbf{M}^{\mathbf{Gal}}{}_{10}$ at P/L = 1/50 with DOPE/DOPC/DOPS = X/(80 − X)/20 membranes was qualitatively similar to that observed for 100% $\mathbf{M}^{\mathbf{Gal}}{}_{10}$. Inverted hexagonal phases and cubic phases were present in membranes with ≥60% DOPE, and lamellar phases were seen in 40% DOPE membranes (Figure 5A,B, see Table S3). However, a notable difference was that, unlike 100% $\mathbf{M}^{\mathbf{Gal}}{}_{10}$, 50% $\mathbf{M}^{\mathbf{Gal}}{}_{10}$ generated negative Gaussian curvature in DOPE/DOPS = 80/20 membranes, as peaks at Q-positions with ratio $\sqrt{3}:\sqrt{4}$ occur, indicating the presence of an *Ia*3*d* "gyroid" cubic phase, which is related to the *Pn*3*m* by a Bonnet transformation.[19] In 50% $\mathbf{M}^{\mathbf{Gal}}{}_{10}$, there are fewer cationic charges, and also more hydrophobic methionine groups compared to 100% $\mathbf{M}^{\mathbf{Gal}}{}_{10}$. The net effect of these changes is a significant expansion of the region of the phase diagram where 50% $\mathbf{M}^{\mathbf{Gal}}{}_{10}$ induces negative Gaussian curvature, and hence can be a potent CPP. Interestingly, the phase behaviors of both 50% $\mathbf{M}^{\mathbf{Gal}}{}_{10}$ and 100% $\mathbf{M}^{\mathbf{Gal}}{}_{10}$ were substantially different from the

DOI: 10.1021/acscentsci.5b00054
ACS Cent. Sci. 2015, 1, 83−88

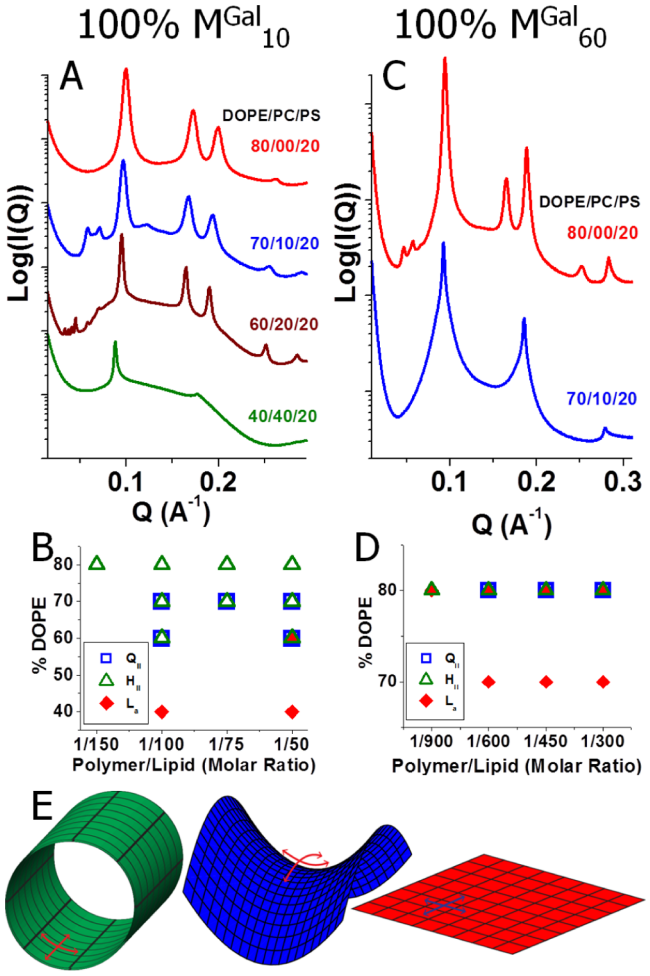

Figure 4. 100% glycosylated $\mathbf{M}^{\mathbf{Gal}}$ polypeptides generate negative Gaussian curvature and negative mean curvature in lipid membranes similar to arginine based cell-penetrating peptides. (A) SAXS spectra of 100% $\mathbf{M}^{\mathbf{Gal}}_{10}$ with DOPE/DOPC/DOPS = X/(80 − X)/20, where X = % DOPE, membranes at peptide to lipid (P/L) = 1/50, molar ratio. In membranes enriched with negative spontaneous curvature lipids, X = 80% DOPE, 100% $\mathbf{M}^{\mathbf{Gal}}_{10}$ generated the inverted hexagonal phase. In reduced PE membranes, X = 70% and 60%, coexisting *Pn3m* cubic and inverted hexagonal phases are present, while a lamellar phase is observed at X = 40%. See Table S3 for lattice parameters of phases. (B) Phase diagram for 100% $\mathbf{M}^{\mathbf{Gal}}_{10}$ with DOPE/DOPC/DOPS membranes as a function of P/L ratio and DOPE content. Overall, nonlamellar inverted hexagonal and cubic phases are observed over a substantial region of the phase diagram. The general phase progression is lamellar, $L_\alpha \rightarrow$ cubic, $Q_{II} \rightarrow$ inverted hexagonal, H_{II}, with increasing membrane DOPE. (C) Analogous SAXS spectra for longer chain 100% $\mathbf{M}^{\mathbf{Gal}}_{60}$ with DOPE/DOPC/DOPS = X/(80 − X)/20 membranes, at P/L = 1/450. Nonlamellar cubic and inverted hexagonal phases are only observed in X = 80% DOPE membranes. (D) Phase diagram for 100% $\mathbf{M}^{\mathbf{Gal}}_{60}$ with DOPE/DOPC/DOPS membranes shows that increasing the chain length strongly reduces the ability of $\mathbf{M}^{\mathbf{Gal}}$ polypeptides to generate negative Gaussian curvature and negative mean curvature. (E) Surfaces with different curvatures. The cylinder (green) has $c_1 < 0$, and $c_2 = 0$ everywhere, so it has negative mean curvature, $H = (1/2)(c_1 + c_2) < 0$, and zero Gaussian curvature, $K = c_1c_2 = 0$. Saddle surfaces (blue) have $c_1 < 0$, and $c_2 > 0$, so they are rich in negative Gaussian curvature, $K < 0$, while a plane (red) has $H = K = 0$ everywhere. Inverted hexagonal phases have cylindrical membrane surfaces, bicontinuous cubic phases have saddle-shaped membrane surfaces, and lamellar phase membranes are flat.

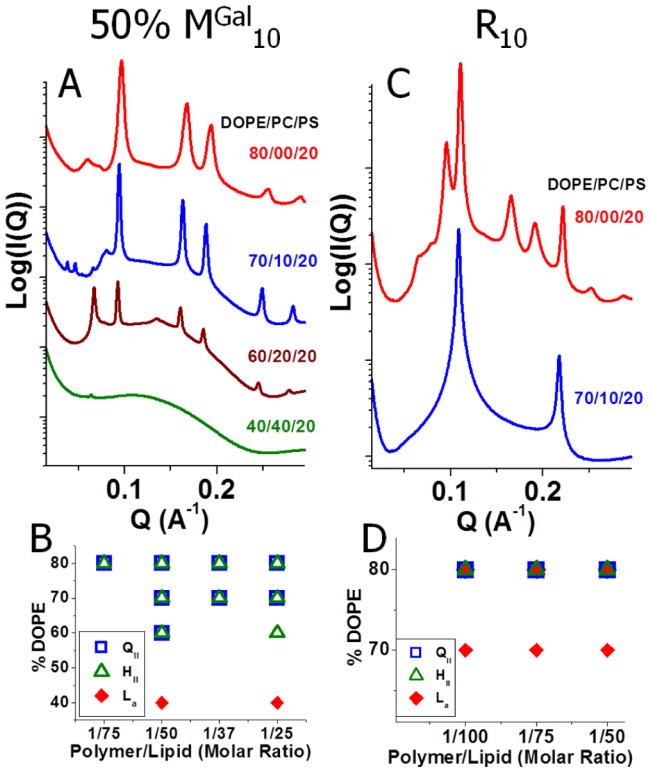

Figure 5. Comparison of phase behavior between 50% glycosylated $\mathbf{M}^{\mathbf{Gal}}_{10}$ and $\mathbf{R}_{10}$ polypeptides. (A) SAXS spectra of 50% $\mathbf{M}^{\mathbf{Gal}}_{10}$ with DOPE/DOPC/DOPS = X/(80 − X)/20 membranes, at P/L = 1/50. Coexisting cubic and inverted hexagonal phases are present in $X \geq$ 60% DOPE membranes, while 50% $\mathbf{M}^{\mathbf{Gal}}_{10}$ displayed negligible ability to restructure X = 40% membranes. (B) Phase diagram of 50% $\mathbf{M}^{\mathbf{Gal}}_{10}$ with DOPE/DOPC/DOPS membranes for different P/L and % DOPE. Overall, this phase diagram is similar to the one for 100% $\mathbf{M}^{\mathbf{Gal}}_{10}$, yet 50% $\mathbf{M}^{\mathbf{Gal}}_{10}$ has a greater ability to generate negative Gaussian curvature over a broader range of membrane compositions. (C) $\mathbf{R}_{10}$ polypeptide at P/L = 1/50 ratio. In X = 70% DOPE, $\mathbf{R}_{10}$ generated lamellar phases, and in 80% DOPE membranes additional *Pn3m* cubic and inverted hexagonal phases are present. (D) Phase diagram for $\mathbf{R}_{10}$ with DOPE/DOPC/DOPS membranes shows that, compared to 50% $\mathbf{M}^{\mathbf{Gal}}_{10}$, $\mathbf{R}_{10}$ generates nonlamellar phases for a smaller range of membrane compositions.

phase behavior of same length poly(L-homoarginine)$_{10}$, $\mathbf{R}_{10}$. $\mathbf{R}_{10}$ was only able to generate nonlamellar *Pn3m* cubic and inverted hexagonal phases in DOPE/DOPS = 80/20 membranes; lamellar phases were observed in membranes with less DOPE (Figure 5C,D). Note that $\mathbf{R}_{10}$ and peptide $\mathbf{R}_9$ showed identical phase behavior under these conditions (see Figure S13). $\mathbf{M}^{\mathbf{Gal}}$ polypeptides, regardless of glycosylation fraction, are thus able to generate negative Gaussian curvature over much broader lipid membrane compositions compared to $\mathbf{R}_{10}$ or $\mathbf{R}_9$.

The ability of $\mathbf{M}^{\mathbf{Gal}}_{10}$ samples to generate both the positive and negative curvature components essential for negative Gaussian curvature is remarkable considering that the molecular structures of $\mathbf{M}^{\mathbf{Gal}}$ polypeptides are substantially different from other known CPPs, which utilize specific amounts of arginine, lysine, and hydrophobicity to generate similar curvatures.[5−7,9] As with other cationic peptides, the high net positive charge of $\mathbf{M}^{\mathbf{Gal}}_{10}$ samples will promote negative membrane curvature, since membrane wrapping maximizes the association between a cationic peptide and an anionic membrane.[8] Unlike conventional arginine based CPPs, however, $\mathbf{M}^{\mathbf{Gal}}_{10}$ samples cannot induce positive membrane curvature through multivalent H-bonding interac-

DOI: 10.1021/acscentsci.5b00054
ACS Cent. Sci. 2015, 1, 83−88

tions with membrane components.[6,20] Instead, we propose that positive curvature arises from constraining the sterically demanding monosaccharides at the lipid membrane, which does not occur with the smaller cationic groups of $\mathbf{M}^{M}$ samples. The volume excluded by the interfacially localized, bulky hydrophilic cations of $\mathbf{M}^{Gal}$ samples can lead to molecular crowding, similar to that observed for concentrated membrane bound proteins,[21] that produces a positive curvature strain on the membrane along the polypeptide chain. A similar mechanism for cell penetration may be involved in certain insect antimicrobial peptides that are known to be highly glycosylated.[22] Since substantial negative Gaussian curvature is generated over a wide range of $\mathbf{M}^{Gal}$ compositions, the glycosylated methionine sulfonium groups in these samples appear to be more potent at generating positive membrane curvature compared to the guanidinium groups in poly(arginine).

The differences in phase behavior observed between 100% $\mathbf{M}^{Gal}_{10}$ and 50% $\mathbf{M}^{Gal}_{10}$ arise from molecular replacement of glycosylated methionine sulfonium cations with hydrophobic methionine groups. In other CPPs, this type of substitution (cationic to hydrophobic) typically results in increased negative Gaussian curvature generation, but with a concomitant increase in cytotoxicity.[6,9] Here, in 50% $\mathbf{M}^{Gal}_{10}$, we also observed increased capacity for negative Gaussian curvature generation, but with an unprecedented decrease in cytotoxicity. This result may be due to the low hydrophobicity of methionine, which is similar to that of alanine in the Eisenberg hydrophobicity scale.[23] In any case, our results exemplify how the essential interactions responsible for membrane permeation can be reproduced and improved without using arginine, by starting with unconventional functionalities in molecular transporters. The sterically demanding glycosylated methionine sulfonium groups found in $\mathbf{M}^{Gal}$ and $\mathbf{M}^{Glc}$ have been identified as a new design motif for creating potent CPPs that transcend the current guanidinium template, and emphasize the generality of curvature generation by molecular transporters as a means to enable their uptake into cells. The reinvention of CPPs using this new motif shows potential for the creation of new CPPs that are highly potent, yet also potentially safe.

METHODS

Preparation of Polypeptides. All α-amino acid *N*-carboxyanhydride (NCA) monomers were synthesized and polymerized using previously described protocols. L-Methionine NCA (Met NCA) was prepared by phosgenation and purified by anhydrous column chromatography.[16] Poly(L-methionine) (poly(Met)) samples, $\mathbf{M}_n$, and 100% methylated, allylated, and benzylated derivatives ($\mathbf{M}^{M}_{60}$, $\mathbf{M}^{A}_{60}$, and $\mathbf{M}^{B}_{60}$) were prepared by polymerization of Met NCA using $(PMe_3)_4Co$ initiator in anhydrous THF or DMF,[24] and then samples were alkylated as previously described.[14] Molecular weights of different poly(Met) were determined by ^{1}H NMR after end-capping samples with α-methoxy-ω-isocyanoethyl-poly(ethylene glycol)$_{22}$ as previously described (see Table S1).[25] Poly(L-homoarginine), $\mathbf{R}_n$, was prepared as previously described via polymerization of N_ε-carboxybenzyl-L-lysine NCA using $(PMe_3)_4Co$ initiator in THF, followed by deprotection with 33% HBr/AcOH in TFA at 0 °C, and then guanylation using 3,5-dimethylpyrazole-1-carboxamidine nitrate in aqueous 1 M NaOH.[26] The guanylation efficiency was >95% determined by ^{1}H NMR. Polypeptide molecular weight and polydispersity were determined by GPC/LS, and ^{1}H NMR of samples end-capped with poly(ethylene glycol)$_{22}$ as described above. Data for the samples used in our experiments are as follows: $\mathbf{R}_{10}$, M_n = 1850, M_w/M_n = 1.09; and $\mathbf{R}_{60}$, M_n = 17,310, M_w/M_n= 1.11. Nona-arginine, $\mathbf{R}_9$, and 100% fluorescein labeled $\mathbf{R}_9$ monodisperse peptides were obtained from Anaspec and were used as received.

MTS Cell Proliferation Assay. The MTS cell proliferation assay (CellTiter 96 AQueous Non-Radioactive Cell Proliferation Assay) was used to quantify any cytotoxic effects of the various polypeptides. The cytotoxicity of the polypeptides was evaluated using HeLa and PC3 cells. Prior to the experiment, 96-well tissue culture plates were seeded at a density of 4×10^4 cells/cm^2 for HeLa cells and 6×10^4 cells/cm^2 for PC3 cells. The polypeptides were prepared in serum-free medium, which lacked FBS, penicillin, and streptomycin, and the polypeptide concentrations were varied. After aspirating the original medium from each well, 100 μL of the prepared medium containing the polypeptides was added to each well and incubated for 5 h in a humidified environment (37 °C, 5.0% CO_2). Following the incubation period, the medium containing polypeptides was aspirated. Subsequently, 20 μL of the MTS reagent was added to each well, and the plate was incubated for an additional 1 h. Cell viability relative to control wells (cells incubated in medium without polypeptides) was quantified by reading the visible light absorbance values at 490 and 700 nm with an Infinite F200 plate reader (Tecan Systems Inc., San Jose, California).

Cellular Uptake Experiments. HeLa and PC3 cells were seeded onto eight-well chambered coverglass units using a cell density of 4×10^4 cells/cm^2 for HeLa cells and 6×10^4 cells/cm^2 for PC3 cells. FITC-labeled polypeptides (ca. 1 mol % label per residue) were diluted in serum-free medium to a concentration of 0.03 mM amino acid. The cells were then incubated with the polypeptides in serum-free medium for 1 or 5 h in a 37 °C humidified atmosphere with 5% CO_2. Following this incubation, the medium was aspirated, and the cells were washed with PBS to remove any polypeptides that were not internalized before the confocal images were taken. Experiments comparing polypeptides of different chain lengths were normalized by use of equivalent amino acid molar concentrations rather than numbers of polypeptide chains.

Laser Scanning Confocal Microscopy (LSCM). LSCM images were taken on a Leica Inverted TCS-SP1MP spectral confocal and multiphoton microscope (Heidelberg, Germany) equipped with an argon laser (476 and 488 nm blue excitation: JDS Uniphase), a diode laser (DPSS; 561 nm yellow-green excitation: Melles Griot), a helium−neon laser (633 nm red excitation), and a two-photon laser setup consisting of a Spectra-Physics Millenia X 532 nm green diode pump laser and a Tsunami Ti-sapphire picosecond pulsed infrared laser tuned at 768 nm for UV excitation. All fluorescence images were obtained using laser scanning confocal microscopy (LSCM), where the images are composed of 0.62 μm thickness, individual *z*-slices of the samples taken from within the cell bodies. While image brightness is not directly comparable between different figures, the LSCM instrument settings were always the same within each figure, allowing meaningful comparisons of fluorescence brightness in any given figure.

SAXS Experiments. Polypeptide and peptide stock solutions were prepared by dissolving the molecules in 100 mM NaCl. Lipids were thoroughly mixed with polypeptides at specific polypeptide to lipid ratios (P/L) in 100 mM NaCl. Sample solutions were hermetically sealed in quartz-glass capillaries (Hilgenberg GmbH, Mark-tubes, code no.: 4017515). Synchrotron SAXS experiments were conducted at the Stanford Synchrotron Radiation Laboratory (BL 4-2). Monochromatic

DOI: 10.1021/acscentsci.5b00054
ACS Cent. Sci. 2015, 1, 83−88

X-rays with 9 keV energy were used. Scattering was collected using a Rayonix MX225-HE detector (pixel size 73.2 μm). Samples were also measured at the California NanoSystems Institute (CNSI) at UCLA. A compact light source (Forvis Technologies, Inc.) was used with a mar345 image plate detector (pixel size 150 μm). Identical samples were prepared and measured at different times and multiple sources to ensure consistency between samples. The 2D SAXS powder patterns were integrated using the Nika 1.48 package (http://usaxs.xray.aps.anl.gov/staff/ilavsky/nika.html) for Igor Pro 6.21 and FIT2D (www.esrf.eu/computing/scientific/FIT2D/).

■ ASSOCIATED CONTENT

Supporting Information

The following file is available free of charge on the ACS Publications website at DOI: 10.1021/acscentsci.5b00054.

Materials and methods, procedures, spectral data, Tables S1−S3, and Figures S1−S13 (PDF)

■ AUTHOR INFORMATION

Corresponding Author

*E-mail: demingt@seas.ucla.edu. Address: Department of Bioengineering, 5121 Engineering 5, HS-SEAS, University of California, Los Angeles, CA 90095. Fax: (+1) 310-794-5956.

Notes

The authors declare no competing financial interest.

‡J.R.K. and N.W.S. contributed equally.

■ ACKNOWLEDGMENTS

This work was supported by a grant from the National Science Foundation (DMR 1308081). Confocal laser scanning microscopy was performed at the CNSI Advanced Light Microscopy/Spectroscopy Shared Resource Facility at UCLA, supported with funding from an NIH-NCRR shared resources grant (CJX1-443835-WS-29646) and NSF Major Research Instrumentation grant (CHE-0722519). SAXS was performed at the Stanford Synchrotron Radiation Lightsource, supported by the U.S. Department of Energy, Basic Energy Sciences, under Contract No. DE-AC02-76SF00515, and at the UCLA CNSI.

■ REFERENCES

(1) Wender, P. A.; Galliher, W. C.; Goun, E. A.; Jones, L. R.; Pillow, T. H. The design of guanidinium-rich transporters and their internalization mechanisms. *Adv. Drug Delivery Rev.* **2008**, *60*, 452−472.

(2) Futaki, S. Membrane-permeable arginine-rich peptides and the translocation mechanisms. *Adv. Drug Delivery Rev.* **2005**, *57*, 547−558.

(3) Brooks, H.; Lebleu, B.; Vivès, E. Tat peptide-mediated cellular delivery: back to basics. *Adv. Drug Delivery Rev.* **2005**, *57*, 559−577.

(4) Mitchell, D. J.; Kim, D. T.; Steinman, L.; Fathman, C. G.; Rothbard, J. B. Polyarginine enters cells more efficiently than other polycationic homopolymers. *J. Pept. Res.* **2000**, *56*, 318−325.

(5) Mishra, A.; et al. Translocation of HIV TAT peptide and analogues induced by multiplexed membrane and cytoskeletal interactions. *Proc. Natl. Acad. Sci. U.S.A.* **2011**, *108*, 16883−16888.

(6) Schmidt, N. W.; et al. Molecular basis for nanoscopic membrane curvature generation from quantum mechanical models and synthetic transporter sequences. *J. Am. Chem. Soc.* **2012**, *134*, 19207−19216.

(7) Mishra, A.; Gordon, V.; Yang, L.; Coridan, R.; Wong, G. C. L. HIV TAT forms pores in membranes by inducing saddle-splay curvature: potential role of bidentate hydrogen bonding. *Angew. Chem., Int. Ed.* **2008**, *47*, 2986−2989.

(8) Schmidt, N.; Mishra, A.; Lai, G. H.; Wong, G. C. L. Arginine-rich cell-penetrating peptides. *FEBS Lett.* **2010**, *584*, 1806−1813.

(9) Schmidt, N. W.; et al. Criterion for amino acid composition of defensins and antimicrobial peptides based on geometry of membrane destabilization. *J. Am. Chem. Soc.* **2011**, *133*, 6720−6727.

(10) Tang, H.; Yin, L.; Kim, K. H.; Cheng, J. Helical poly(arginine) mimics with superior cell-penetrating and molecular transporting properties. *Chem. Sci.* **2013**, *4*, 3839−3844.

(11) Ornelas-Megiatto, C.; Wich, P. R.; Fréchet, J. M. J. Polyphosphonium polymers for siRNA delivery: an efficient and nontoxic alternative to polyammonium carriers. *J. Am. Chem. Soc.* **2012**, *134*, 1902−1905.

(12) Hemp, S. T.; Allen, M. H., Jr.; Green, M. D.; Long, T. E. Phosphonium-containing polyelectrolytes for nonviral gene delivery. *Biomacromolecules* **2012**, *13*, 231−238.

(13) Hemp, S. T.; Allen, M. H., Jr.; Smith, A. E.; Long, T. E. Synthesis and properties of sulfonium polyelectrolytes for biological applications. *ACS Macro Lett.* **2013**, *2*, 731−735.

(14) Chakraborty, S.; et al. Ternary nylon-3 copolymers as host-defense peptide mimics: beyond hydrophobic and cationic subunits. *J. Am. Chem. Soc.* **2014**, *136*, 14530−14535.

(15) Kramer, J. R.; Deming, T. J. Preparation of multifunctional and multireactive polypeptides via methionine alkylation. *Biomacromolecules* **2012**, *13*, 1719−1723.

(16) Kramer, J. R.; Deming, T. J. Reversible chemoselective tagging and functionalization of methionine containing peptides. *Chem. Commun.* **2013**, *49*, 5144−5146.

(17) Kramer, J. R.; Deming, T. J. A general method for purification of α-amino acid-*N*-carboxyanhydrides using flash chromatography. *Biomacromolecules* **2010**, *11*, 3668−3672.

(18) Zimmerberg, J.; Kozlov, M. M. How proteins produce cellular membrane curvature. *Nat. Rev. Mol. Cell Biol.* **2006**, *7*, 9−19.

(19) Shearman, G. C.; Ces, O.; Templer, R. H.; Seddon, J. M. Inverse lyotropic phases of lipids and membrane curvature. *J. Phys.: Condens. Matter* **2006**, *18*, S1105−S1124.

(20) Cui, Q.; Zhang, L. L.; Wu, Z.; Yethiraj, A. Generation and sensing of membrane curvature: Where materials science and biophysics meet. *Curr. Opin. Solid State Mater. Sci.* **2013**, *17*, 164−174.

(21) Stachowiak, J. C.; et al. Membrane bending by protein−protein crowding. *Nat. Cell Biol.* **2012**, *14*, 944−949.

(22) Bulet, P.; Hetru, C.; Dimarcq, J.-L.; Hoffmann, D. Antimicrobial peptides in insects; structure and function. *Dev. Comp. Immunol.* **1999**, *23*, 329−344.

(23) Eisenberg, D.; Weiss, R. M.; Terwilliger, T. C.; Wilcox, W. Hydrophobic moments and protein structure. *Faraday Symp. Chem. Soc.* **1982**, *17*, 109−120.

(24) Deming, T. J. Cobalt and iron initiators for the controlled polymerization of α-amino acid-N-carboxyanhydrides. *Macromolecules* **1999**, *32*, 4500−4502.

(25) Brzezinska, K. R.; Curtin, S. A.; Deming, T. J. Polypeptide end-capping using functionalized isocyanates: preparation of pentablock copolymers. *Macromolecules* **2002**, *35*, 2970−2976.

(26) Rodriguez, A. R.; Choe, U.-J.; Kamei, D. T.; Deming, T. J. Fine tuning of vesicle assembly and properties using dual hydrophilic triblock copolypeptides. *Macromol. Biosci.* **2012**, *12*, 805−811.

DOI: 10.1021/acscentsci.5b00054
ACS Cent. Sci. 2015, 1, 83−88